

Spin pumping in YIG-Pt structures: the role of the van Hove singularities

Y.V. Nikulin^{1,2}, Y.V. Khivintsev^{1,2}, M.E. Seleznev^{1,2}, S.L. Vysotskii^{1,2}, A.V. Kozhevnikov¹,
V.K. Sakharov^{1,2}, G.M. Dudko¹, A. Khitun³, S.A. Nikitov⁴, Y.A. Filimonov^{1,2,5*}

¹Kotelnikov Institute of Radioengineering and Electronics of RAS, Saratov Branch, Saratov, Russia, 410019

²Saratov State University, Saratov, Russia, 410032

³Department of Electrical and Computer Engineering, University of California -Riverside, Riverside, California, USA 92521

⁴Kotelnikov Institute of Radioengineering and Electronics of RAS, Moscow, Russia, 125009

⁵Yuri Gagarin State Technical University of Saratov, Saratov, Russia, 410054

*yuri.a.filimonov@gmail.com

Abstract Spin pumping by surface and backward volume magnetostatic waves in YIG/Pt structures is experimentally studied and analyzed. It is shown that at frequencies corresponding to van Hove singularities in the density of states of the spin wave spectrum, an increase in the efficiency of electron-magnon scattering and spin current generation takes place. The obtained results are important for spin wave-based spintronic devices development.

Key words: YIG/Pt structures, spin pumping, magnon density of states

Angular momentum transfer in magnetic multilayer structures plays a central role in spintronic physics and devices. Of significant interest from the point of view of creating energy-efficient devices are structures based on ferromagnetic insulators and heavy metals with strong spin-orbit interaction, where angular momentum currents or spin currents are transferred by spin waves (SW) or magnons [1-7]. In such structures, the exchange interaction of conduction electrons with spins localized at the insulator-metal interface and spin-orbit interaction leads to spin-dependent electron-magnon scattering and spin current transport through the interface. As one of the basic structures of insulator magnon spintronics, structures based on films of yttrium iron garnet ($\text{Y}_3\text{Fe}_5\text{O}_{12}$ (YIG)) and platinum (Pt) [1-6] are considered, which is due to extremely low SW damping in YIG and a sufficiently large spin Hall angle in Pt. In YIG/Pt structures, due to the spin Hall effect [7], it is possible to convert the electric current in Pt into SW in YIG [8,9] and control their propagation [10-12]. On the other hand, due to the inverse spin Hall effect (ISHE), it is possible to detect the spin current injected into the Pt film through the interface during spin pumping by both incoherent [8,13-17] and coherent SWs upon excitation of ferromagnetic resonance (FMR) [18-22] or SWs propagation [23-25] and interference [26].

The spin current J_s transferred through a unit surface area of the YIG/Pt interface is determined by the difference in the reflectivity of the interface with respect to electrons with opposite spin orientations during electron-magnon scattering processes [27]. The value of J_s is proportional to the number of scattering channels, which is characterized by the number of magnetic Fe ions exchange-coupled with Pt electrons on the YIG surface and is determined by the choice of technological process parameters that affect the roughness, elemental composition and microstructure of the interface [28-35]. On the other hand, the value of J_s reflects the intensity of electron-magnon scattering processes in each of the channels and is determined by the parameters of the interacting electron and magnon subsystems. Within the framework of an approach to describing electron-magnon scattering in YIG/Pt structures based on the sd-model, it was shown [36,37] that one of the parameters of the magnon subsystem that determines the spin current J_s through the interface is the density of states in the spectrum of spin waves $\rho(\omega)$:

$$J_s \sim \int \Omega(\omega) \cdot \rho(\omega) d\omega, \quad (1)$$

where $\Omega(\omega)$ contains a statistical factor characterizing the distribution of magnons and electrons, and information on the rates of inelastic transitions involving excited magnons at frequency ω . In experiments on spin pumping by coherent SWs, the connection between J_s and $\rho(\omega)$ can play a significant role in cases where the SW frequency $f = \omega/2\pi$ coincides with the frequency f^* corresponding to the van Hove singularity frequency ($\rho(f^*) \rightarrow \infty$) [38] in the density of states of the SW spectrum of the YIG film. In the case of the pump frequency f^* , we should expect a resonant increase in $J_s(f^*)$ and, as a consequence, a resonant increase in the electromotive force (EMF) $V_{ISHE}(f^*)$ generated due to the inverse spin Hall effect ($V_{ISHE} \sim J_s$). In this letter, we report on the experimental observation of the effect of a resonant increase in the efficiency of spin pumping at frequencies of van Hove singularities in the density of states of spin waves.

The typical geometry for a spin pump experiment in thin-film YIG/Pt structures assumes that the external magnetic field \vec{H} lies in the plane of the structure. The SW spectrum for a tangentially magnetized film consists of the surface (MSSW) and backward volume (BVMSW) magnetostatic waves [39]. BVMSWs with the wave vector $\vec{k} \parallel \vec{H}$ occupy the frequency range $[f_H, f_0]$, where $f_0 = \sqrt{f_H^2 + f_H f_m}$, $f_H = \gamma H$, $f_m = \gamma 4\pi M$, $\gamma = 2.8 \text{ MHz/Oe}$ is gyromagnetic ratio for YIG, $4\pi M = 1750 \text{ G}$ is YIG magnetization. MSSW at $\vec{k} \perp \vec{H}$ occupy the frequency band $[f_0, f_s]$, where $f_s = f_H + f_m/2$. The frequency dependences of the density of states in the spectrum of the BVMSW ($\rho_v(f)$) and MSSW ($\rho_s(f)$) can be written in the form [39]:

$$\rho_v(f) = \frac{f f_m}{f_H \sqrt{f_0^2 - f^2}}, \quad \rho_s(f) = \frac{f_H}{\sqrt{f^2 - f_0^2}} \cdot \frac{1}{\sqrt{2(f^2 - f_H^2) - f_H f_m - 2f \sqrt{f^2 - f_0^2}}}. \quad (2)$$

The density of states in the spectrum of the BVMSW has a singularity ($\rho_v(f_0) \rightarrow \infty$) at the frequency f_0 of the long-wavelength ($k \rightarrow 0$) spectrum limit, which coincides with the frequency of the uniform FMR. In the case of MSSW, the singularity in the density of states is achieved at frequencies f_0 and f_s , where f_s corresponds to the short-wave ($k \rightarrow \infty$) boundary of the spectrum.

In order to experimentally confirm the correlation of the frequency dependences $\rho_s(f)$ and $V_{ISHE}(f)$ and, thereby, to approve the determinant contribution of singularities to the efficiency of electron-magnon scattering, it is convenient to make the experiment in the presence of two frequencies of van Hove singularities f_0 and f_s in the MSSW spectrum. In this case, to observe the correlation between $V_{ISHE}(f)$ and $\rho_s(f)$, which has the form (2), it is necessary to fulfill a number of requirements both for the parameters of YIG films and for the experimental parameters. Firstly, the relation $2d > l^{ex}$ must be satisfied between the thickness d of YIG films and the free path length of the exchange SW l^{ex} in order to minimize the influence of inhomogeneous exchange interaction on the MSSW dispersion [40,41] and obtain the dependence $\rho_s(f)$ of the form (2). For typical epitaxial YIG films, the condition $2d > l^{ex}$ is satisfied at a thickness $d \geq 8 \mu\text{m}$ [41,42].

Secondly, it is necessary to ensure the excitation of MSSW in the entire frequency band $[f_0, f_s]$, which is realized when using microstrip SW antennas with a width w less than the thickness d of the YIG film ($w < d$) [43]. Finally, the low Volt-Watt sensitivity S of YIG/Pt structures ($S < 10^{-2} \text{ V/W}$) [15,19] forces experimentation at bias fields $H > 2\pi M = 875 \text{ Oe}$, when three-magnon (3M) processes of decay are prohibited for MSSW over the entire frequency band $[f_0, f_s]$, and cannot limit the power of MSSW [44,45]. Therefore, in the work, the results obtained at $H = 939 \text{ Oe}$ are considered.

In our experiment, we studied spin pumping by MSSW and BVMSW in the structures based on a YIG film having area covered by Pt film between a pair of the strip line microantennas (MA) integrated on the YIG surface, see Fig. 1. Several samples based on YIG films epitaxially grown on gadolinium gallium garnet (GGG) substrates with the planar dimensions of $15\text{ mm} \times 15\text{ mm}$ were fabricated using magnetron sputtering, photolithography, and ion etching. Each sample contained a set of the YIG/Pt-MA structures with a different distance between MA and Pt area dimensions. MAs made out of $0.5\ \mu\text{m}$ thick copper were $250\ \mu\text{m}$ long and $4\ \mu\text{m}$ wide. MAs with contact pads (designated Roman I and II in Fig. 1) for connecting microwave microprobes, as well as contacts to Pt, were made in the same technological step. Pt films had a thickness of 4 to 10 nm, a width of $200\ \mu\text{m}$, and a length of $200\text{--}800\ \mu\text{m}$. The samples were placed in the electromagnet gap so that the in-plane magnetic field \vec{H} was directed along ($\vec{k} \perp \vec{H}$) or perpendicular ($\vec{k} \parallel \vec{H}$) to the MAs. The geometry $\vec{k} \perp \vec{H}$ corresponds to the excitation of MSSWs with dispersion law $f(k)$ [32]:

$$f^2 = f_0^2 + \frac{f_m^2}{4}(1 - e^{-2kd}). \quad (3)$$

SWs characteristics were measured using a vector network analyzer. Measurements of the frequency dependencies of the EMF $V_{ISHE}(f)$ were carried out in the mode of modulation of the incident microwave power P_{in} with a frequency of 11 kHz. Most of the experiments were performed with structures based on YIG films grown on GGG substrates with crystallographic orientation (111) and thickness $d = 8; 11; 14; 20$ and $41\ \mu\text{m}$. To clarify the nature of the influence of YIG crystallographic anisotropy, we also used a film with $d = 16\ \mu\text{m}$ grown on a GGG substrate with crystallographic orientation (100). It turned out that for the considered YIG/Pt structures, neither a change in the crystallographic orientation of the substrate nor a change in the YIG thickness introduces fundamental changes in the character of the $V_{ISHE}(f)$ dependences. The results for the YIG(8 μm)/Pt(8nm)/GGG(111) structure will be considered below.

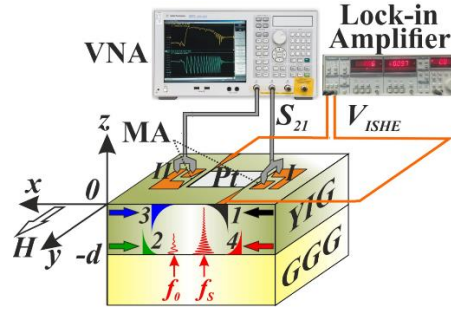


Figure 1. Scheme of the experiment and studied YIG/Pt structure. Roman I and II show strip line microantennas (MA) with contact pads for microwave probes, 3 and 4 contact pads to the Pt film for measuring EMF. In the inset, the color distribution of the fields of the dipole MSSW corresponding to curves 1-4 in Fig. 2c is shown in color. Oscillating lines schematically show partial volume exchange waves at frequencies f_0 ($l^{ex} < d$) and f_s ($l^{ex} \sim d$), at the YIG/GGG boundary.

The results presented in Fig. 2 illustrate the character of the frequency dependences of the MSSW signal transmission coefficient $S_{12}(f)$, the dispersion dependence $k = k(f)$, the conversion coefficient $K(f)$ of the input power P_{in} into the MSSW power P and the EMF $V_{ISHE}(f)$ in the studied structures. Vertical dotted lines in Fig. 2 show the position of the long-wavelength $f_0 = 4.43\text{ GHz}$ and short-wavelength $f_s = 5.09\text{ GHz}$ limits of the dipole MSSW spectrum, calculated using (3) for the selected field value $H = 939\text{ Oe}$. From Fig. 2 it can be seen that the frequency range in which the transmission of the MSSW and the generation of EMF is observed, as well as

the measured dependence $k = k(f)$ correspond to the Damon-Eschbach MSSW [39]. In this case, in the dependence $V_{ISHE}(f)$, it is possible to identify maxima near the frequencies f_0 and f_s , which at the applied power $P_{in} = -5 \text{ dBm}$ are $V_{ISHE}(f_0) \cong 70 \text{ nV}$ and $V_{ISHE}(f_s) \cong 130 \text{ nV}$, Fig. 2c. This behavior of $V_{ISHE}(f)$ cannot be explained by the frequency dependence of the coefficient $K(f)$, which, in our case, smoothly increases with frequency from values $K(f) \approx 0.2$ to values $K(f) \approx 0.6$, see Fig. 2b. Therefore, it should be assumed that an increase in the values of $V_{ISHE}(f)$ at frequencies f_0 and f_s reflects an increase in the efficiency of electron-magnon scattering at the interface at these frequencies. The dotted curve in Fig. 2c shows the dependence $\rho_s(f)$, calculated using (2) It can be seen that the frequencies f_0, s , at which EMF maxima are observed, correspond to the frequencies of van Hove singularities in the density of states $\rho_s(f)$ in the spectrum of dipole MSSWs.

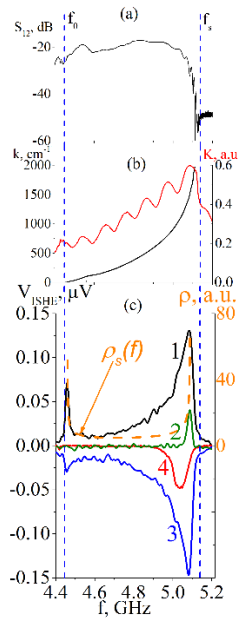


Figure.2 Case of MSSW $\vec{k} \perp \vec{H}$. Frequency dependences of: (a) transmission magnitude $S_{12}(f)$; (b) the wave number $k=k(f)$ and the coefficient of conversion of the incident power P_{in} into the MSSW power $K(f)$; (c) $V_{ISHE}(f)$ generated for $P_{in} \approx -5 \text{ dBm}$ – solid line and $\rho_s(f)$ calculated using formula (2) – dotted line; (d) $V_{ISHE}(f)$ obtained when changing the direction of the magnetic field \vec{H} and/or the direction of propagation of MSSW \vec{k} to the opposite, where curves 1, 3 and 2, 4 correspond to the propagation of MSSW along the YIG/Pt and YIG/GGG boundaries, respectively. Vertical dotted lines show the position of the long-wave (f_0) and short-wave (f_s) limits of the MSSW spectrum. Structure YIG(8 μm)/Pt(8nm)/GGG(111), $H \approx 939 \text{ Oe}$.

To show that the measured EMF is due to the injection of spin current through the YIG/Pt interface, let us consider the $V_{ISHE}(f)$ dependences obtained for the opposite directions of the magnetic field \vec{H} and/or the directions of propagation of the MSSW \vec{k} that are indicated by numbers 1-4 in Fig. 2s. Curves 1 and 2 correspond to the direction of \vec{H} , shown by the arrow in Fig. 1, while curves 3 and 4 correspond to the opposite direction of \vec{H} . Dependences 1(3) correspond to cases when antenna I(II) is taken as the input and the MSSW propagates along the YIG/Pt boundary. Curves 2(4) correspond to the case when antenna II(I) is taken as the input and the MSSW propagates along the YIG/GGG boundary. From the results presented in Fig. 4, it follows that the sign of the generated EMF is determined by the direction of \vec{H} , while a change in the direction of \vec{k} at a constant \vec{H} affects the signal magnitude due to the non-reciprocity of MSSW propagation.

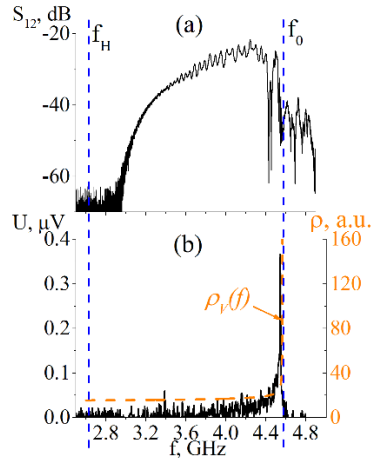


Figure 3. Case of BVMSW $\vec{k} \parallel \vec{H}$. Frequency dependences of: (a) transmission magnitude $S_{12}(f)$; (b) $V_{ISHE}(f)$ for $P_{in} \approx -5$ dBm – the solid line and $\rho_v(f)$ calculated using formula (2) – dotted line. Structure YIG(8 μ m)/Pt(8nm)/GGG(111), $H \approx 939$ Oe.

Figure 3 shows the results obtained for the case of the propagation of BVMSW ($\vec{k} \parallel \vec{H}$ – geometry) in the structure. It can be seen that BVMSWs propagate in the frequency band 2.9 GHz – 4.43 GHz, which is in good agreement with the theoretical interval $[f_H, f_0]$, see Fig. 3a. From Fig. 3b it can be seen that, in this case, the signal $V_{ISHE}(f)$ is observed only near the frequency f_0 . In this case, the character of the frequency dependence of $V_{ISHE}(f)$ is consistent with the calculation using formula (2) of the dependence $\rho_v(f)$, which is shown in Fig. 3b with a dotted line.

For the case of MSSW, it is necessary to discuss the differences in the character of the frequency dependence of the results of the calculation of $\rho_s(f)$ and the measurements of $V_{ISHE}(f)$, shown in Fig. 2c. First of all, note the faster growth with frequency $V_{ISHE}(f)$, compared to $\rho_s(f)$. The reason for this may be the hybridization of the dipole MSSW with the exchange volume waves of the film, which have the dispersion law $f^2 = \tilde{f}_H^2 + \tilde{f}_H f_m$, where $\tilde{f}_H = f_H + f_{ex}$, $f_{ex} = f_m \alpha Q^2$, $Q^2 = k^2 + k_{\perp}^2$, $\alpha = 3 \cdot 10^{-12}$ cm² is exchange constant in YIG [46,47]. Projections of the group velocity $\vec{v}_g = 2\pi \nabla_{\vec{q}} f$ of such SWs onto the plane $v_g^{\parallel}(f)$ and the normal $v_g^{\perp}(f)$ of the film can be written in the form $v_g^{\parallel}(f) = 4\pi \alpha k f_m \beta$ and $v_g^{\perp}(f) = 4\pi \alpha k_{\perp} f_m \beta$, where $\beta = (\tilde{f}_{ex} + f_s)/f \sim 1$. At $k \rightarrow 0$, the component $v_g^{\parallel}(f) \rightarrow 0$, which is typical for dispersion regions with a high density of states [38]. The coupling of the MSSW with exchange waves increases with the wave number k [46,47] and increases the density of states at frequencies $f_0 < f < f_s$ due to the hybridization of the spectra of the dipole MSSW with exchange waves having a high density of states.

The noted hybridization effects can be associated with a significant difference in the EMF values at frequencies f_0 and f_s for MSSW propagating along the YIG/GGG boundary, see curves 2 and 4 in Fig. 2d. Indeed, in our case, near the frequency f_0 for exchange SWs, the following estimates are valid: $k_{\perp} = \pi/d \approx 4 \cdot 10^3$ cm⁻¹, $v_g^{\perp}(f_0) < 7 \cdot 10^2$ cm/s, $d \gg l^{ex}(f_0) = \frac{v_g^{\perp}(f_0)}{2\pi f_0 \bar{\alpha}} \leq 1 \mu\text{m}$, where $\bar{\alpha} \sim 3 \cdot 10^{-4}$ is the relaxation parameter in YIG [1]. At frequency $f_s = 5.09$ GHz $k_{\perp} \approx 50\pi/d \approx 2 \cdot 10^4$ cm⁻¹, $v_g^{\perp}(f_s) > 10^4$ cm/s and exchange SWs have $l^{ex}(f_s) \approx 9 \mu\text{m} \sim d$. In the inset to Fig. 1, two red oscillating curves illustrate the path length of exchange SWs at frequencies f_0 and f_s . As a result, at frequency f_s , a larger number of SWs excited by MSSW at the interface with the GGG substrate can reach the YIG/Pt interface and participate in electron-magnon scattering processes. It should be noted that the proposed explanation does not take into account the change in the effective magnetization $4\pi M^{ef}(z)$ across the film thickness, which can

significantly affect not only the efficiency of hybridization of MSSWs with exchange modes, but also the position of the “turning points” corresponding to the places of effective generation of exchange SWs by the MSSW field relatively to the film boundaries [48].

When comparing the character of the dependences $V_{ISHE}(f)$ and $\rho_s(f)$ near the long-wave limit of the MSSW spectrum, it is necessary to take into account that magnetic anisotropy fields in the vicinity of f_0 can lead to the appearance of anisotropic volume magnetostatic waves (AVMSW) in the spectrum of the film [49]. In the spectrum of such AVMSWs, taking into account the inhomogeneous exchange, dispersion regions can additionally be formed, where the group velocity of the SW is $v_g(f) \rightarrow 0$ and a singularity in the density of states arises.

It should be noted that the spin conductivity of the YIG/Pt interface is influenced only by those van Hove singularities for which a high density of states in the SW spectrum is achieved precisely at the interface. In the case when the SW singularities are localized in the volume of the YIG film at the singularity frequency, their contribution to the spin conductivity of the interface will be small. An example of such a singularity can be the frequency of the “bottom” $f_{bot} \cong \tilde{f}_H$ in the spectrum of a tangentially magnetized film, since the population of the “bottom” of the spectrum by parametric SWs under the conditions of 3M decay processes of the pump MSSW with a frequency $f_p > 2f_{bot}$ is not accompanied by the appearance of the signal $V_{ISHE}(f)$ [50].

Thus, using the example of spin pumping by traveling magnetostatic waves in YIG/Pt structures, the relationship between the efficiency of spin current transport through the interface and van Hove singularities in the density of states of the spin wave spectrum of the structure is shown. The increase in the spin conductivity of the interface is due to an increase in the efficiency of electron-magnon scattering at singularity frequencies. It should be noted that at frequencies of van Hove singularities, simultaneously with the density of states, the effective mass of magnons increases, which should also enhance the process of electron scattering [51]. The obtained results open a new approach for the design of spintronic structures with effective spin current pumping by propagating spin waves. Besides that, the obtained results may be useful for the development of spintronics structures in which effective spin transport is carried out by SW with the required frequency and wavelength, which is important for the miniaturization of devices. In turn, in addition to the frequencies f_0 and f_s in the SW spectrum, van Hove singularities can be formed at frequencies f^* of various resonant interactions leading to the formation an additional sections with $v_g(f^*) \rightarrow 0$ in the dispersion law. An example of such frequencies f^* can be the frequencies of Bragg resonances [52] as well dipole-exchange resonances in single [53] and exchange-coupled [54] YIG films. Note also that the high sensitivity of electron-magnon scattering to van Hove singularities is similar to photon-magnon scattering in the Mandelstam-Brillouin spectroscopy method [55]. However, the mechanism for the occurrence of EMF is associated with spin-wave excitations having a high density of states on the surface, while the intensity of light scattering has an integral characteristic over the film volume.

Funding

This work was supported by the Russian Science Foundation under grant 22-19-00500. The work of Nikitov S.A. was carried out within the framework of the state task "Spintronics". The work of A. Khitun was supported in part by the National Science Foundation (NSF) under Award # 2006290, Program Officer Dr. S. Basu and by the INTEL CORPORATION (Award #008635, Spin Wave Computing) (Project director is Dr. D. E. Nikonov).

Conflict of interest.

The authors declare that they have no conflict of interest.

References

1. A.Chumak, V. Vasyuchka, A. Serga, B. Hillebrands. Magnon spintronics. *Nature Phys* **11**, 453–461 (2015). <https://doi.org/10.1038/nphys3347>
2. V.E. Demidov, S. Urazhdin, G. de Loubens, O. Klein, V. Cros, A. Anane, S.O. Demokritov. Magnetization oscillations and waves driven by pure spin currents. *Phys. Rep.* **673**, 23 (2017) <http://dx.doi.org/10.1016/j.physrep.2017.01.001>
3. M. Althammer. Pure spin currents in magnetically ordered insulator/normal metal heterostructures. *J. Phys. D: Appl. Phys.* **51**, 313001 (2018); DOI:10.1088/1361-6463/aaca89
4. V.E. Demidov, S. Urazhdin, A. Anane, V. Cros, S. O. Demokritov. Spin–orbit-torque magnonics. *Journal of Applied Physics* **127**, 170901 (2020); <https://doi.org/10.1063/5.0007095>
5. A. Brataas, B. van Wees, O. Klein, G. de Loubens, M. Viret. Spin insulatronics. *Physics Reports*, **885**, 1 (2020); <https://doi.org/10.1016/j.physrep.2020.08.006>
6. S.A. Nikitov, A.R. Safin, D.V. Kalyabin, A.V. Sadovnikov, E.N. Beginin, M.V. Logunov, M.A. Morozova, S.A. Odintsov, S.A. Osokin, A.Yu. Sharaevskaya, Yu.P. Sharaevsky, A.I. Kirilyuk. Dielectric magnonics: from gigahertz to terahertz. *Phys. Usp.* **63**, 945–974 (2020); <https://doi.org/10.3367/UFNe.2019.07.038609>
7. J. Sinova, S. O. Valenzuela, J. Wunderlich, C. H. Back, T. Jungwirth. Spin Hall effects. *Rev. Mod. Phys.* **87**, 1213 (2015) <https://doi.org/10.1103/RevModPhys.87.1213>
8. Y. Kajiwara, K. Harii, S. Takahashi, J. Ohe, K. Uchida, M. Mizuguchi, H. Umezawa, H. Kawai, K. Ando, K. Takanashi, S. Maekawa, E. Saitoh. Transmission of electrical signals by spin-wave in-ter-conversion in a magnetic insulator// *Nature* **464**, 262 (2010); doi: 10.1038/nature08876
9. M. Collet, X. de Milly, O. d’Allivy Kelly, V. V. Naletov, R. Bernard, P. Bortolotti, J. Ben Youssef, V. E. Demidov, S. O. Demokritov, J. L. Prieto, M. Muñoz, V. Cros, A. Anane, G. de Loubens, O. Klein. Generation of coherent spin-wave modes in yttrium iron garnet microdiscs by spin–orbit torque. *Nat Commun.* **7**, 10377 (2016). <https://doi.org/10.1038/ncomms1037720>.
10. Z. Wang, Y. Sun, M. Wu, V. Tiberkevich, A. Slavin. Control of Spin Waves in a Thin Film Ferromagnetic Insulator through Interfacial Spin Scattering. *Phys. Rev. Lett.* **107**, 146602 (2011); <https://doi.org/10.1103/PhysRevLett.107.146602>
11. E. Padrón-Hernández; A. Azevedo; S. M. Rezende. Amplification of spin waves in yttrium iron garnet films through the spin Hall effect. *Appl. Phys. Lett.* **99**, 192511 (2011); <https://doi.org/10.1063/1.3660586>
12. M. Evelt, V. E. Demidov, V. Bessonov, S. O. Demokritov, J. L. Prieto, M. Muñoz, J. Ben Youssef, V. V. Naletov, G. de Loubens, O. Klein, M. Collet, K. Garcia-Hernandez, P. Bortolotti, V. Cros, A. Anane. High-efficiency control of spin-wave propagation in ultra-thin yttrium iron garnet by the spin-orbit torque. *Appl. Phys. Lett.* **108**, 172406 (2016); <https://doi.org/10.1063/1.4948252>
13. K.-I. Uchida, H. Adachi, T. Ota, H. Nakayama, S. Maekawa, E. Saitoh. Observation of longitudinal spin-Seebeck effect in magnetic insulators. *Appl. Phys. Lett.* **97**, 172505 (2010); <https://doi.org/10.1063/1.3507386>
14. C. W. Sandweg, Y. Kajiwara, A. V. Chumak, A. A. Serga, V. I. Vasyuchka, M. B. Jungfleisch, E. Saitoh, B. Hillebrands, Spin Pumping by Parametrically Excited

- Exchange Magnons. Phys. Rev. Lett. **106**, 216601 (2011); <https://doi.org/10.1103/PhysRevLett.106.216601>
15. H. Kurebayashi, O. Dzyapko, V. E. Demidov, D. Fang, A. J. Ferguson S. O. Demokritov. Controlled enhancement of spin-current emission by three-magnon splitting. Nature Materials, **10**, 660 (2011); <https://doi.org/10.1038/NMAT3053>
 16. H. Kurebayashi, O. Dzyapko, V. E. Demidov, D. Fang, A. J. Ferguson, S. O. Demokritov, Spin pumping by parametrically excited short-wavelength spin waves. Appl. Phys. Lett. **99**, 162502 (2011); <https://doi.org/10.1063/1.3652911>
 17. T. B. Noack, V. I. Vasyuchka, D. A. Bozhko, B. Heinz, P. Frey, B. Hillebrands, A. A. Serga. Enhancement of the Spin Pumping Effect by Magnon Confluence Process in YIG/Pt Bilayers. Phys. Status Solidi B **256**, 1900121 (2019); DOI: 10.1002/pssb.201900121
 18. M. Agrawal; A.A. Serga; V. Lauer; E.Th. Papaioannou; B. Hillebrands; V.I. Vasyuchka. Microwave-induced spin currents in ferromagnetic-insulator|normal-metal bilayer system. Appl. Phys. Lett. **105**, 092404 (2014); <https://doi.org/10.1063/1.4894636>
 19. C.W. Sandweg, Y. Kajiwara, K. Ando, E. Saitoh, B. Hillebrands. Enhancement of the spin pumping efficiency by spin wave mode selection Appl. Phys. Lett. **97**, 252504 (2010); <https://doi.org/10.1063/1.3528207>
 20. V. Castel, N. Vlietstra, J. Ben Youssef, B. J. van Wees. Platinum thickness dependence of the inverse spin-Hall voltage from spin pumping in a hybrid yttrium iron garnet/platinum system. Appl. Phys. Lett. **101**, 132414 (2012); <https://doi.org/10.1063/1.4754837>
 21. V. Castel, N. Vlietstra, B. J. van Wees, and J. Ben Youssef. Frequency and power dependence of spin-current emission by spin pumping in a thin-film YIG/Pt system. Phys. Rev. B **86**, 134419 (2012); <https://doi.org/10.1103/PhysRevB.86.134419>
 22. M. B. Jungfleisch, A. V. Chumak, A. Kehlberger, V. Lauer, D. H. Kim, M. C. Onbasli, C. A. Ross, M. Klaui, B. Hillebrands. Thickness and power dependence of the spin-pumping effect in Y3Fe5O12/Pt heterostructures measured by the inverse spin Hall effect. Phys. Rev. B, **91**, 134407 (2015); <https://doi.org/10.1103/PhysRevB.91.134407>
 23. A.V. Chumak, A. A. Serga, M. B. Jungfleisch, R. Neb, D. A. Bozhko, V. S. Tiberkevich, B. Hillebrands. Direct detection of magnon spin transport by the inverse spin Hall effect. Appl. Phys. Lett. **100**, 082405 (2012); <https://doi.org/10.1063/1.3689787>
 24. O. d'Allivy Kelly, A. Anane, R. Bernard, J. Ben Youssef, C. Hahn, A H. Molpeceres, C. Carré-téro, E. Jacquet, C. Deranlot, P. Bortolotti, R. Lebourgeois, J.-C. Mage, G. de Loubens, O. Klein, V. Cros, A. Fert. Inverse spin Hall effect in nanometer-thick yttrium iron garnet/Pt system. Appl. Phys. Lett. **103**, 082408 (2013); <https://doi.org/10.1063/1.4819157>
 25. M. Balinsky, M. Ranjbar, M. Haidar, P. Dürrenfeld, R. K. Dumas, S. Khartsev, A. Slavin, J. Åkerman. Spin pumping and the inverse spin Hall effect via magnetostatic surface spin-wave modes in YIG/Pt bilayers. IEEE Magn. Lett., **6**, 3000604 (2015); DOI: 10.1109/LMAG.2015.2471276
 26. M. Balinskiy, H. Chiang, D. Gutierrez, A. Khitun. Spin wave interference detection via inverse spin Hall effect. Appl. Phys. Lett. **118**, 242402 (2021); <https://doi.org/10.1063/5.0055402>
 27. Y. Tserkovnyak, A. Brataas, G.E.W. Bauer. Enhanced Gilbert Damping in Thin Ferromagnetic Films. Phys. Rev. Lett. **88**, 117601 (2002); <https://doi.org/10.1103/PhysRevLett.88.117601>
 28. Z. Qiu, K. Ando, K. Uchida, Y. Kajiwara, R. Takahashi, H. Nakayama, T. An, Y. Fujikawa, E. Saitoh. Spin mixing conductance at a well-controlled platinum/yttrium iron garnet interface. Appl. Phys. Lett. **103**, 092404 (2013); <https://doi.org/10.1063/1.4819460>

29. Y. Saiga, K. Mizunuma, Y. Kono, J. C. Ryu, H. Ono, M. Kohda, E. Okuno, Platinum thickness dependence and annealing effect of the spin-Seebeck voltage in platinum/yttrium iron garnet structures. *Appl. Phys. Express*, **7**, 093001 (2014). <https://doi.org/10.7567/APEX.7.093001>
30. L. Liu, Y. Li, Y. Liu, T. Feng, J. Xu, X. R. Wang, D. Wu, P. Gao, J. Li. Interfacial modulation of spin pumping in YIG/Pt. *Phys. Rev. B* **102**, 014411 (2020); doi:10.1103/PhysRevB.102.014411
31. D. Song, L. Ma, S. Zhou, J. Zhu. Oxygen deficiency induced deterioration in microstructure and magnetic properties at Y₃Fe₅O₁₂/Pt interface. *Appl. Phys. Lett.* **107**, 042401 (2015); <https://doi.org/10.1063/1.4927551>
32. M. B. Jungfleisch, V. Lauer, R. Neb, A. V. Chumak, B. Hillebrands. Improvement of the yttrium iron garnet/platinum interface for spin pumping-based applications. *Appl. Phys. Lett.* **103**, 022411 (2013); <https://doi.org/10.1063/1.4813315>
33. Y. Sun, H. Chang, M. Kabatek, Y-Y. Song, Z. Wang, M. Jantz, W. Schneider, M. Wu, E. Montoya, B. Kardasz, B. Heinrich, S. G. E. te Velthuis, H. Schultheiss, A. Hoffmann. Damping in Yttrium Iron Garnet Nanoscale Films Capped by Platinum. *Phys. Rev. Lett.* **111**, 106601 (2013); <https://doi.org/10.1103/PhysRevLett.111.106601>
34. A. Aqeel, I. J. Vera-Marun, B. J. van Wees, T. T. M. Palstra. Surface sensitivity of the spin Seebeck effect. *J. Appl. Phys.* **116**, 153705 (2014); <https://doi.org/10.1063/1.4897933>
35. D. Song, L. Ma, S. Zhou, J. Zhu. Oxygen deficiency induced deterioration in microstructure and magnetic properties at Y₃Fe₅O₁₂/Pt interface. *Appl. Phys. Lett.* **107**, 042401 (2015); <https://doi.org/10.1063/1.4927551>
36. S. Takahashi, E. Saitoh, S. Maekawa. Spin current through a normal-metal/insulating-ferromagnet junction. *J. Phys.: Conf. Series* **200**, 062030 (2010); DOI 10.1088/1742-6596/200/6/062030
37. E.G. Tveten, A. Brataas, Y. Tserkovnyak. Electron-magnon scattering in magnetic heterostructures far out of equilibrium. *Phys. Rev. B*, **92**, 180412(R) (2015); <https://doi.org/10.1103/PhysRevB.92.180412>
38. L. van Hove. The Occurrence of Singularities in the Elastic Frequency Distribution of a Crystal. *Physical Review*, **89**, 1189 (1953); <https://doi.org/10.1103/PhysRev.89.1189>
39. R. W. Damon, J. R. Eshbach, Magnetostatic modes of a ferromagnet slab. *J. Phys. Chem. Solids*, **19**, 308 (1961); doi:10.1016/0022-3697(61)90041-5
40. R. E. De Wames, T. Wolfram. Dipole-Exchange Spin Waves in Ferromagnetic Films. *J. Appl. Phys.* **41**, 987 (1970); <https://doi.org/10.1063/1.1659049>
41. Gulyaev Yu. V., Bugaev A. S., Zil'berman P. E., Ignat'ev I. A., Konovalov A. G., Lugovskoi A. V., Mednikov A. M., Nam B. P., Nikolaev E. I. Giant oscillations in the transmission of quasi-surface spin waves through a thin yttrium-iron garnet (YIG) film. *JETP Lett.* **30**, 565 (1979); http://jetpletters.ru/ps/1368/article_20705.pdf
42. Gulyaev Yu.V., Zil'berman P.E., Lugovskoi A.V. The influence of inhomogeneous exchange and dissipation on the propagation of Damon-Eschbach surface waves in a ferromagnetic plate. *Sov. Phys.-Solid State* **23**, 660 (1981)
43. Gurevich AG, Melkov GA. *Magnetization Oscillations and Waves*. Boca Raton: CRC Press; 1996. 464 p
44. Kazakov G. T., Kozhevnikov A. V., Filimonov Y. A. Four-magnon decay of magnetostatic surface waves in yttrium iron garnet films. *Physics of the Solid State*. **39**, 288-295 (1997); DOI: 10.1134/1.1129801.

45. Kazakov G. T., Kozhevnikov A. V., Filimonov Y. A. The effect of parametrically excited spin waves on the dispersion and damping of magnetostatic surface waves in ferrite films. *Journ. Exper. Theor. Phys.* **88**, 174-181 (1999); DOI: 10.1134/1.558780.
46. T. Wolfram, R.E. De Wames. Linewidth and dispersion of the virtual magnon surface state in thick ferromagnetic films. *Phys. Rev. B*, **1**, 4358 (1970); <https://doi.org/10.1103/PhysRevB.1.4358>
47. G.T. Kazakov, A.G. Sukharev, Yu.A. Filimonov. Exchange radiative losses of Damon-Eshbach surface magnetostatic waves in YIG-films. *Fizika Tverdogo Tela (Leningrad)* **32**, 3571-357 (1990)
48. P. E. Zil'berman, A. G. Temiryazev, M. P. Tikhomirova, "Short spin waves of exchange nature in ferrite films: Excitation, propagation, and potential applications," *Phys.-Usp.* **38**(10), 1173–1177 (1995); <https://doi.org/10.1070/pu1995v038n10abeh001493>
49. P.E. Zil'berman, V.M. Kulikov, V.V. Tikhonov, I.V. Shein. Nonlinear effects in the propagation of surface magnetostatic waves in yttrium iron garnet films in weak magnetic fields. *JETP*, **72**(5), 874 (1991); http://www.jetp.ras.ru/cgi-bin/dn/e_072_05_0874.pdf
50. Seleznev ME, Nikulin YV, Khivintsev YV, Vysotskii SL, Kozhevnikov AV, Sakharov VK, Dudko GM, Pavlov ES, Filimonov YA. Influence of three-magnon decays on electromotive force generation by magnetostatic surface waves in integral YIG – Pt structures. *Izvestiya VUZ. Applied Nonlinear Dynamics.* **30**(5):617– 643 (2022) DOI: 10.18500/0869-6632-003008
51. J.A. Reissland. *The Physics of Phonons*. John Wiley & Sons, Ltd (1973).
52. Vysotskii S.L., Nikitov S.A., Filimonov Y.A. Magnetostatic spin waves in two-dimensional periodic structures (magnetophoton crystals). *J. Exp. Theor. Phys.* **101**, 547–553 (2005). <https://doi.org/10.1134/1.2103224>
53. M.E. Seleznev, Yu.V. Nikulin, V.K. Sakharov, Yu.V. Khivintsev, A.V. Kozhevnikov, S.L. Vysotskiy, Yu.A. Filimonov. Influence of the resonant interaction of surface magnetostatic waves with exchange modes on the EMF generation in YIG/Pt structures. *Technical Physics*, **92**, 2074 (2022); DOI: 10.21883/TP.2022.13.52224.136-21
54. S. Vysotskii, A. Kozhevnikov, M. Balinskiy, A. Khitun, Y. Filimonov. Giant sensitivity to magnetic field variation in the spin wave interferometer based on the system of exchange-coupled films of yttrium iron garnet. *J. Appl. Phys.* **132**, 084504 (2022); <https://doi.org/10.1063/5.0102336>
55. R. E. Camley, T. S. Rahman, D. L. Mills Magnetic excitations in layered media: Spin waves and the light-scattering spectrum. *Phys. Rev. B* **27**, 261 (1983); <https://doi.org/10.1103/PhysRevB.27.261>

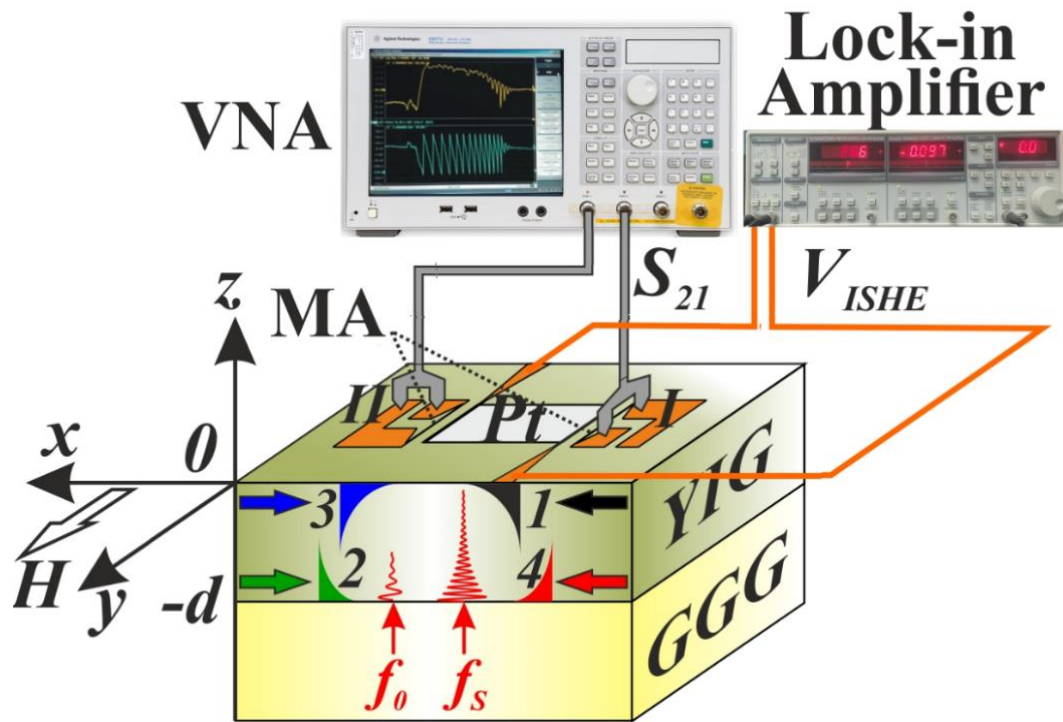


Figure 1. Scheme of the experiment and studied YIG/Pt-MA structure. Roman I and II show strip line antennas with contact pads for microwave probes, 3 and 4 contact pads to the Pt film for measuring EMF. In the inset, the color distribution of the fields of the dipole MSSW corresponding to curves 1-4 in Fig. 2c is shown in color. Oscillating lines schematically show partial volume exchange waves at frequencies f_0 ($l^{ex} < d$) and f_s ($l^{ex} \sim d$), at the YIG/GGG boundary.

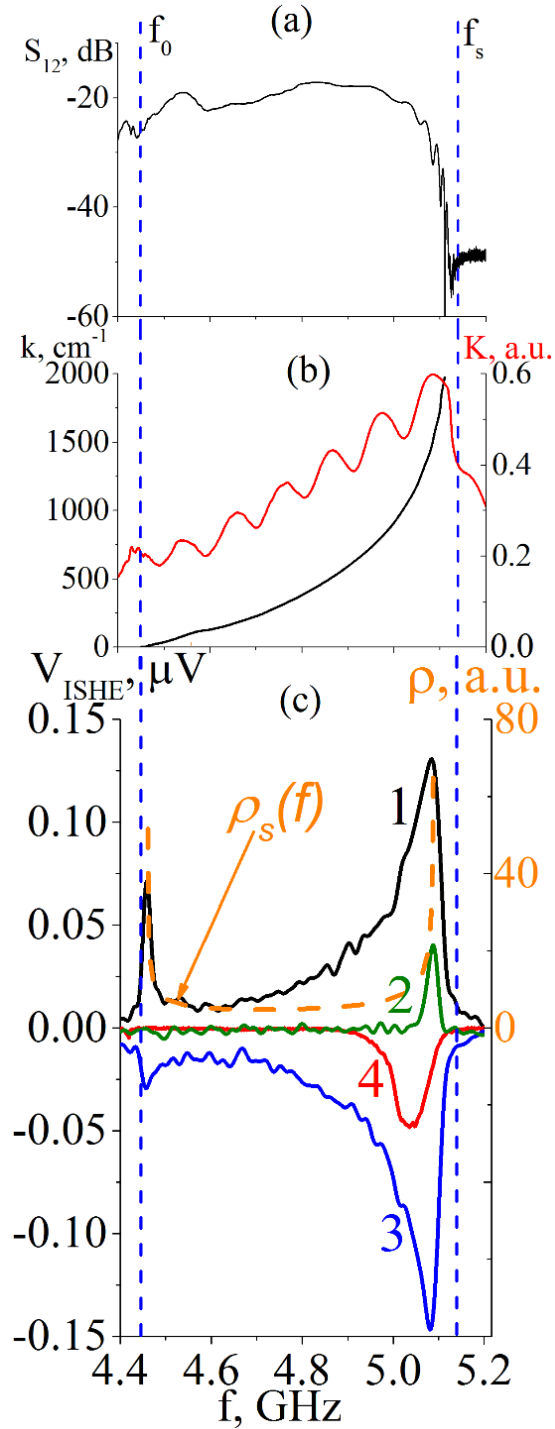


Figure.2 Case of MSSW $\vec{k} \perp \vec{H}$. Frequency dependences of: (a) transmission magnitude $S_{12}(f)$; (b) the wave number $k=k(f)$ and the coefficient of conversion of the incident power P_{in} into the MSSW power $K(f)$; (c) $V_{ISHE}(f)$ generated for $P_{in} \approx -5 \text{ dBm}$ – solid line and $\rho_s(f)$ calculated using formula (2) – dotted line; (d) $V_{ISHE}(f)$ obtained when changing the direction of the magnetic field \vec{H} and/or the direction of propagation of MSSW \vec{k} to the opposite, where curves 1, 3 and 2, 4 correspond to the propagation of MSSW along the YIG/Pt and YIG/GGG boundaries, respectively. Vertical dotted lines show the position of the long-wave (f_0) and short-wave (f_s) limits of the MSSW spectrum. Structure YIG(8 μm)/Pt(8nm)/GGG(111), $H \approx 939 \text{ Oe}$.

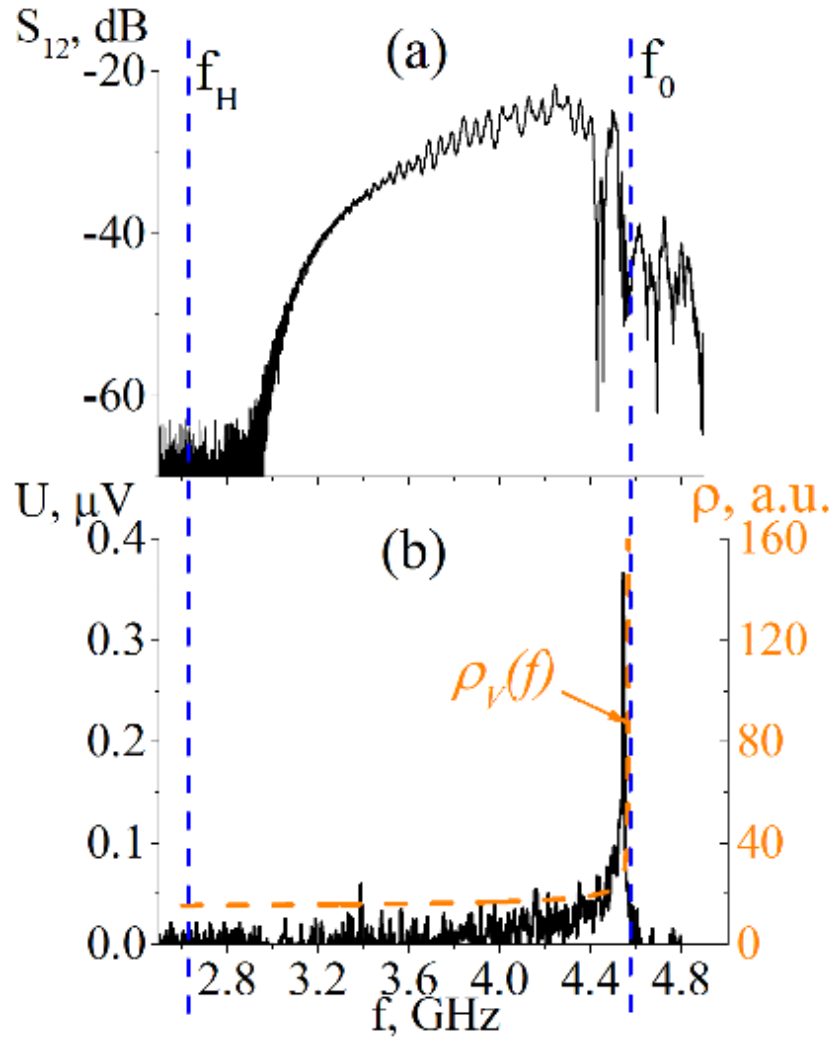


Figure 3. Case of BVMSW $\vec{k} \parallel \vec{H}$. Frequency dependences of: (a) transmission magnitude $S_{12}(f)$; (b) $V_{ISHE}(f)$ for $P_{in} \approx -5$ dBm – the solid line and $\rho_v(f)$ calculated using formula (2) – dotted line. Structure YIG(8 μ m)/Pt(8nm)/GGG(111), $H \approx 939$ Oe.